Hindawi
Advances in Civil Engineering
Volume 2021, Article ID 6614391, 12 pages
https://doi.org/10.1155/2021/6614391

Research Article

Influence of Acidic Substances on Compression Deformation Characteristics of Loess

Hao Tang,[1,2] **Chiyang Liu**,[1,2] **Nianqin Wang**,[1,2] **Huahua Li**,[1,2] **Guannan Wu**,[1,2] **Jinzhi Luo**,[1,2] **and Mengli Zeng**[1,2]

[1]*College of Geology and Environment, Xi'an University of Science and Technology, Xi'an 710054, China*
[2]*Shaanxi Provincial Key Laboratory of Geological Support for Coal Green Exploitation, Xi'an University of Science and Technology, Xi'an 710054, China*

Correspondence should be addressed to Chiyang Liu; 18209074021@stu.xust.edu.cn

Received 8 December 2020; Revised 6 April 2021; Accepted 8 April 2021; Published 20 April 2021

Academic Editor: Valeria Vignali

Current research theories on acid-contaminated soils indicate that acids can alter the physical properties of soils, which in turn can affect their engineering mechanical properties. However, compressibility, one of the most important mechanical properties of loess, may be affected by acidic substances. To investigate the influence of acid on the compression properties of loess, this study uses a uniaxial compressor to investigate the changes of compression properties of loess under different acid concentrations and different acid immersion times and attempts to predict the causes of macroscopic compressibility changes from the microscopic pore changes of acid-etched loess. The test results show that when the soaking time is the same, the hydrochloric acid concentration increases from 0 to 3.0 mol/L, the compression coefficient C_c increases by 43.20–87.5%, and the compression yield stress σ_{pc} decreases by 51.36–60.86%; when the concentration of hydrochloric acid is the same, the soaking time increases from 1 day to 12 days, the compression coefficient C_c increases by 119.05–197.46%, and compressive yield stress σ_{pc} decreases by 10.67–22.02%. The microscopic images of loess soaked for 12 days at 3.0 mol/L hydrochloric acid concentration were compared with those of the original loess. The percentages of micropore, small pore, mesopore, and macropore areas of original loess were 20.90%, 79.10%, 0%, and 0%, respectively. The percentages of micropore, small pore, mesopore, and macropore areas of acid-etched loess were 6.24%, 37.21%, 1.14%, and 55.40%, respectively. The enhancement of the compressive properties of acid-etched loess is the result of the coupling of acid concentration and soaking time, and the change of macroscopic compressive properties may be related to the increase of microscopic macropore area after acid erosion. The results of this study can be used as a reference for the study of soil mechanical properties in acid-contaminated soils.

1. Introduction

Loess sediments result from wind-formed accumulation and consist mainly of fine sand and clay, rich in calcium carbonate [1]. Loess is found in Asia, Europe, South America, and parts of North America [2–5]. There is an area of 631,000 km^2 of soil in China that is covered by loess, and properties such as loose and porous loess, vertical joint development, and water sensitivity make the loess engineering studies complex [6]. Meanwhile, these areas are prone to produce a series of loess natural and secondary disasters, such as landslides [7–11]. The properties exhibited by loess under the influence of external forces, which mainly include the compression and shear resistance of loess, that is, the deformation and strength characteristics of loess, are an important part of the engineering properties of loess, which are related to the stability and safe use of engineered buildings.

The compressibility of loess refers to its ability to deform in compression with volume reduction under pressure, which is mainly due to the extrusion of water and gas in the pores under the action of external pressure. The solid particles of loess move close to each other, and the pores between particles gradually reduce.

Compressibility testing of loess is usually carried out indoors using a uniaxial compressor. A parametric relationship between the porosity ratio of loess and stress is used to convert and characterize the compressibility of loess, and a loess CCC is plotted from the loess confined compression test (CCT), wherein the CCC generally has two distinct regions that can be approximated by two straight lines [12, 13], one being the swelling curve (SL) and the other being the virgin compression line (VCL). The intersection of the two curves, namely, the CCC and SL, is called the compressive yield stress, which is also called the prior consolidation pressure for natural structural loams, where SL characterizes the elasticity of the loam and VCL characterizes the plasticity of the loam [14, 15], By calculating the slope of the VCL, it is possible to obtain the compression index C_c, which is an important indicator of the compressibility of constant-volume loess. The higher the compression index, the more compressible the soil [16–19]. The level of compressibility of loess soil is determined by its own properties, including its particle size composition, mineral composition, structural configuration, water content, and density. Further, it is also governed by external environmental factors, such as the amount of external pressure, rate of pressurization, dynamic load action, acidic and alkaline substances, and temperature.

With an increase in urbanization and industrialization, the acidic and alkaline wastewater produced by factory enterprises change the physical and mechanical properties of the soil [20–22]. Chemical wastewater from industries infiltrates into the soil, thereby causing serious pollution. This pollution involves complex chemical reactions between the soil and pollutants, thus changing the properties of the soil in different environments. Among these, acidic pollution leads to a number of problems, such as structural aspects of the soil, bulging of slabs, and foundations [23, 24]. Such acidic contaminants may originate from metal leaching, petroleum refining, paper industry, and dye factories. Chemical contaminants leak into the ground and may cause deformation of foundations, and acids can react violently with carbonate materials in loess to produce salts, carbon dioxide, and water. Carbonate materials in loess predominantly contribute to its chemical properties, and the physical and mechanical properties of loess may change when acidic substances enter the loess [25, 26].

In this study, we investigated the compressive properties of loess under different concentrations of hydrochloric acid and different immersion times of acid in a compressed chamber. In addition, we studied the effect of acid on the pore size of loess with the help of a scanning electron microscope.

2. Materials and Methods

2.1. Sample Preparation. Loess materials were obtained from the toe of a slope in Lintong County, Xi'an City, Shaanxi Province. These samples are tawny, rich in vertical joints, and low in natural moisture content, and show good uniformity and high levels of compaction. The basic physical properties of the loess test results are listed in Table 1. The specific gravity, natural density, and water content of the soil, carried out in accordance with Standard GB/T 50123, were 2.68, 16.5 kN/m^3, and 17.6%, respectively. The liquid and plastic limits were measured as $\omega_L = 31.3\%$ and $\omega_P = 19.4\%$, respectively. All samples of natural undisturbed loess were made with standard ring cutters on-site, and the required size was 79.8 mm in diameter and 20 mm in height. For the undisturbed loess ring knife sample prepared in the field environment, it was sealed with plastic wrap, placed in a sealed box, appropriately stored, and transported to the laboratory.

The following test was conducted on the loess sample: the undisturbed loess ring knife sample taken from the sampling site was immersed in a hydrochloric acid solution, and the acid-contaminated erosion sample under normal laboratory conditions was simulated. Before soaking in the acid solution, the samples were wrapped and numbered. A schematic diagram of the sample design and the physical drawing is shown in Figure 1. The upper and lower sides of the sample were pasted with filter paper with medium permeability, and two permeable stones were added. The most outer part of the sample is wrapped with corrosion-resistant polypropylene cloth and tied tightly with rubber bands. The purpose is to make the acid evenly penetrate into the soil sample during the soaking process, and the soil particles will not disintegrate and lose.

The processed samples were soaked solutions that consisted of equal volumes of distilled water and hydrochloric acid solutions with concentrations of 0.1, 0.5, 1, 2, and 3 mol/L. The soaking times were 1, 3, 6, 9, and 12 days, with a total of 30 samples, as shown in Figure 1. The container used for preparing the hydrochloric acid immersion solution was a glass beaker of 500 mL, and the volume of immersion solution corresponding to each concentration was 200 mL.

2.2. Confined Compression Test (CCT). The test in this study was performed using a single lever triplex high-pressure oedometer at the Xi'an University of Science and Technology, China. The test procedures for all mechanical tests followed these standards [27–29].

A rapid compression method was used to perform the compression test on acid-etched samples. Then, they were weighed prior to the CCT. Vertical normal stresses, σ, of 50, 100, 200, 300, and 400 kPa were applied sequentially. Each stress was applied for 60 min and the displacement (accuracy ± 0.01 mm) was read at the end of each loading interval (without recovery). The standard for compression stability is that the vertical displacement of the sample within two hours is less than 0.002 mm.

When the CCT was completed, the samples were dried in an oven at 105°C for at least 48 h and weighed again to determine the water content and bulk density. From the recorded displacement, d, the void ratio, e, was calculated as

$$e = \frac{\rho_s}{\rho_d} \frac{H_0 - d}{H_0} - 1, \quad (1)$$

where ρ_s is the particle density, ρ_d is the initial bulk density, and H_0 is the initial height of the loess.

Table 1: Physical property index of the natural undisturbed loess samples.

Water ratio ω (%)	Natural density ρ (g/cm^3)	Specific gravity G_s	Liquid limit ω_L (%)	Plastic limit ω_p (%)	Plastic index I_p (%)	Liquidity index I_L (%)
17.6	16.5	2.68	31.3	19.4	12	−0.15

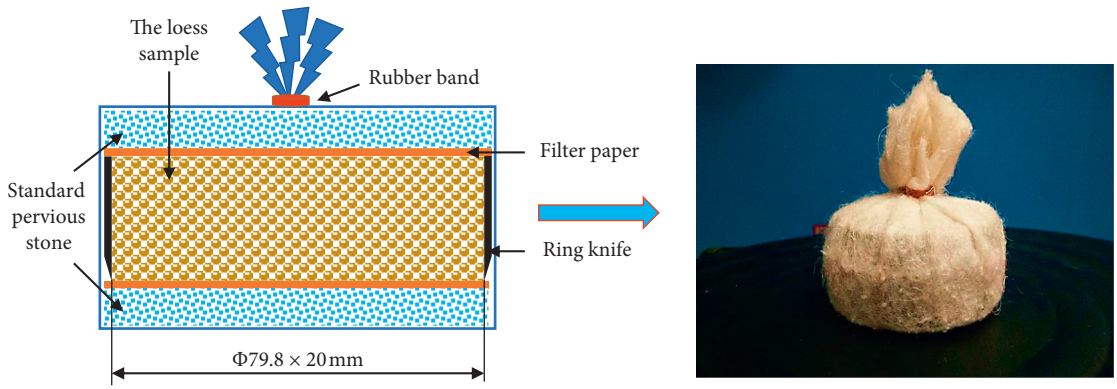

Figure 1: Schematic diagram of sample and object. (a) Test soil sample design. (b) Sample drawing.

The compressive behaviour of soil, represented by the CCC, is then expressed in a semi-logarithmic diagram, that is, as a relationship between the logarithm of applied stress, σ, and the void ratio, e. When expressed in an $e - \log\sigma$ diagram, the compaction characteristic has two distinct regions that can be approximated by two lines: the swelling (or recompression) line (SL) and the VCL. This approximation represents an elastoplastic model. The point of intersection between SL and VCL is referred to as the precompression stress, σ_{pc}. The compression curve contains three important soil compression properties: the swelling or recompression index, C^s, the compression index, C^c, and the precompression stress, σ^{pc}, where C^s is equal to the slope of the SL and C^c is equal to the slope of the VCL. Experimental soil compression data (σ, e) were fitted to the Gompertz [30] equation as proposed by Gregory et al. [26] using nonlinear least squares fitting:

$$e = a + c\ \exp\{-[b(\log\ \sigma - \xi)]\}, \tag{2}$$

where a, b, c, and ξ are adjustable parameters, and log is the logarithm function to the base of 10.

The precompression stress, σ_{pc}, was estimated as the stress at maximum curvature of the compression curve. Note that this will result in slightly lower values for σ_{pc} when compared to the values obtained using the Casagrande [31] method. The curvature function, κ, is given by Gregory et al. [26]:

$$\kappa = \frac{d^2e/d(\log\ \sigma)^2}{\left[1 + (de/d(\log\ \sigma))^2\right]^{3/2}}, \tag{3}$$

where the first and second derivatives of equation (2) are given as follows:

$$\frac{de}{d\log\ \sigma} = [bc\ \exp(-(\exp(b(\log\ \sigma - \xi))))] \cdot [-\exp(b(\log\ \sigma - \xi))], \tag{4}$$

$$\frac{d^2e}{d(\log\ \sigma)^2} = \left[b^2c\ \exp(-(\exp(b(\log\ \sigma - \xi))))\right] \cdot [\exp(b(\log\ \sigma - \xi))]\,[\exp(b(\log\ \sigma - \xi)) - 1]. \tag{5}$$

The maximum κ and the corresponding σ (i.e., σ at maximum $\kappa = \sigma_{pc}$) were then determined numerically.

2.3. SEM Tests. To investigate the corrosion characteristics of acid on loess microscopic pores, a sample containing undisturbed loess and another sample that has been corroded by 3 mol/L of strong hydrochloric acid for 12 days were prepared. Those samples were placed in a drying oven (the temperature was set to 105°C; the time was 8 h), and the drying was complete. The sample was carefully cut with a knife into a cylindrical sample with a diameter of 2 cm and a height of 2 cm. In order to increase the hardness of the sample and obtain better scanning results, a curing agent was slowly dropped into the sample to solidify and harden the sample. The curing agent was composed of epoxy resin, acetone, ethylenediamine, and phthalic acid. In the butyl ester solution (100 : 200 : 6 : 2), the complete curing agent penetrated the sample, and it was allowed to dry naturally at room temperature for 48 h to fully cure the sample. A polishing machine was used to grind and polish the surface to be scanned. In order to increase the conductivity of the

sample soil, ion sputtering of platinum (Pt) was implemented. Image collection was carried out using a Quanta FEG scanning electron microscope system, manufactured by the American FEI company. Thereafter, image processing was performed using the publicly available software program, namely, Particles (Pores) and Cracks Analysis System (PCAS) [32, 33].

3. Results and Discussion

3.1. Confined Compression Curve (CCC). The acid-etched loess is compressed by the acid concentration and soaking time; the converted porosity e and the vertical load σ are determined. Further, the half logarithmic coordinate curve $e - \log \sigma$ is plotted, and the curve is the CCC of acid-etched loess (Figure 2).

For an acid immersion time of 1 day (Figure 2(a)), the initial pore ratio e_0 of the sample was different for different acid concentrations, which showed that as the acid concentration increased (0–3.0 mol/L), the initial pore ratio e_0 of the sample increased, and the position of the CCC also showed a certain regularity; the higher the acid concentration, the higher the position of the CCC. As the immersion time increased, the distance between the CCC of the samples for each acid concentration also widened. The spacing between the curves in Figure 2(e) is significantly wider than that in Figure 2(b). For the same acid concentration, the CCC of the samples increased with increasing immersion time and the higher position of the curves, as shown in Figures 3(f)–3(j).

3.2. Compression Index C_c. The value of the compression index C_c can be calculated from the slope of the VCL in the CCC. We considered the sample CCC with a soaking time of 12 days and an acid concentration of 3 mol/L as an example to calculate the compression index C_c value, as shown in Figure 3. We calculated the slope d of VCL to be −0.423 and considered the absolute value of the slope d to obtain the value of the compression index C_c of the sample. According to this method, the compression index C_c value and the compression index C_c of the remaining groups of samples (hydrochloric acid concentrations of 0.1, 0.5, 1.0, 2.0, and 3.0 mol/L, immersion times of 1, 3, 6, 9, and 12 days) were sequentially calculated. These values are listed in Table 2.

It can be seen from Table 2 that, for the sample immersed in the acid solution for 1 day, as the acid solution concentration increased from 0.1 mol/L to 3.0 mol/L, the compression index C_c value increased from 0.118 to 0.210; the increase, which is ΔC_c, was 0.092, and the increase ratio was 177.97%. For the acid solution immersed for 12 days, as the acid concentration increased from 0.1 mol/L to 3.0 mol/L, the compression index C_c value increased from 0.351 to 0.460; the increase, that is, ΔC_c, was 0.109, and the increase ratio was 131.05%. From another perspective, the sample with a concentration of 0.1 mol/L immersed in an acid solution, as the immersion time increased from 1 day to 12 days, the value of the compression index C_c increased from 0.118 to 0.351; the increase in ΔC_c was 0.233, and the increase ratio was 297.46%. Finally, the sample with an acid concentration of 3.0 mol/L was immersed. As the immersion concentration increased from 1 day to 12 days, the value of the compression index C_c increased from 0.210 to 0.460, the increase in ΔC_c was 0.250, and the increase ratio was 219.05%. It can be concluded that as the immersion time increased and the acid concentration increased, the compression index C_c of loess gradually increased. This increase in value could be attributed to the coupling of the acid concentration and the immersion time.

To characterize the influence of the acid concentration and immersion time on the change in the compression index of loess samples, the compression index C_c values listed in Table 2 were linearly fitted to obtain the result shown in Figure 4, and the fitting equation is provided in Table 3. The horizontal axis is the acid concentration, and the vertical axis is the compression index C_c. It can be seen from the figure that the linear relationship between the sample compression index C_c and the acid concentration showed a positive correlation. The acid concentration ranges from 0.1, 0.5, 1.0, 2.0, and 3.0 mol/L gradually increased, and the corresponding compression index values (C_c) also increased with a positive correlation. The range of equation fit R^2 was between 0.811 and 0.952. The horizontal axis is the number of immersion days t, and the vertical axis is the compression index C_c. The result of linear fitting of the data points is shown in Figure 5. The linear relationship between the compression index C_c of the sample and the immersion time showed a positive correlation. The fitting equation is provided in Table 3. The immersion times were gradually increased from 1, 3, 6, 9, and 12 days, and the corresponding compression index values (C_c) also increased in a positive relationship, and the R^2 range of the fitted equation was between 0.652 and 0.858.

3.3. Compressive Yield Stress σ_{pc}. The value of the compressive yield stress σ_{PC} is generally determined by the intersection of the swelling line (SL) and the CCC. As shown in Figure 6, the value of the initial consolidation stress P_c of the undisturbed loess was similar to the value at this point. To determine the compressive yield stress, initially, the angular bisector of the horizontal asymptote and SL is determined; the intersection of the VCL and this angular bisector is Q, and the abscissa of Q is the value of the desired compressive yield stress. The value corresponding to this inflection point of acid-corroded loess is considered to be a turning point of the soil sample's elasticity to plasticity, and it is also considered to be the failure point of the soil compression structure, which is of great significance to the study of the compression characteristics of acid-corroded loess. Because the method of determining the compressive yield stress by the method of intersection of the SL and CCC tangents is subjective in the selection of the tangent, it is subjectively chosen to approximate the line segment between, and hence, there is still a certain error. This study intends to use the mathematical nonlinear fitting method, wherein the parameters of equation (2) are determined; then, the first and second derivatives (equations (3) and (4))

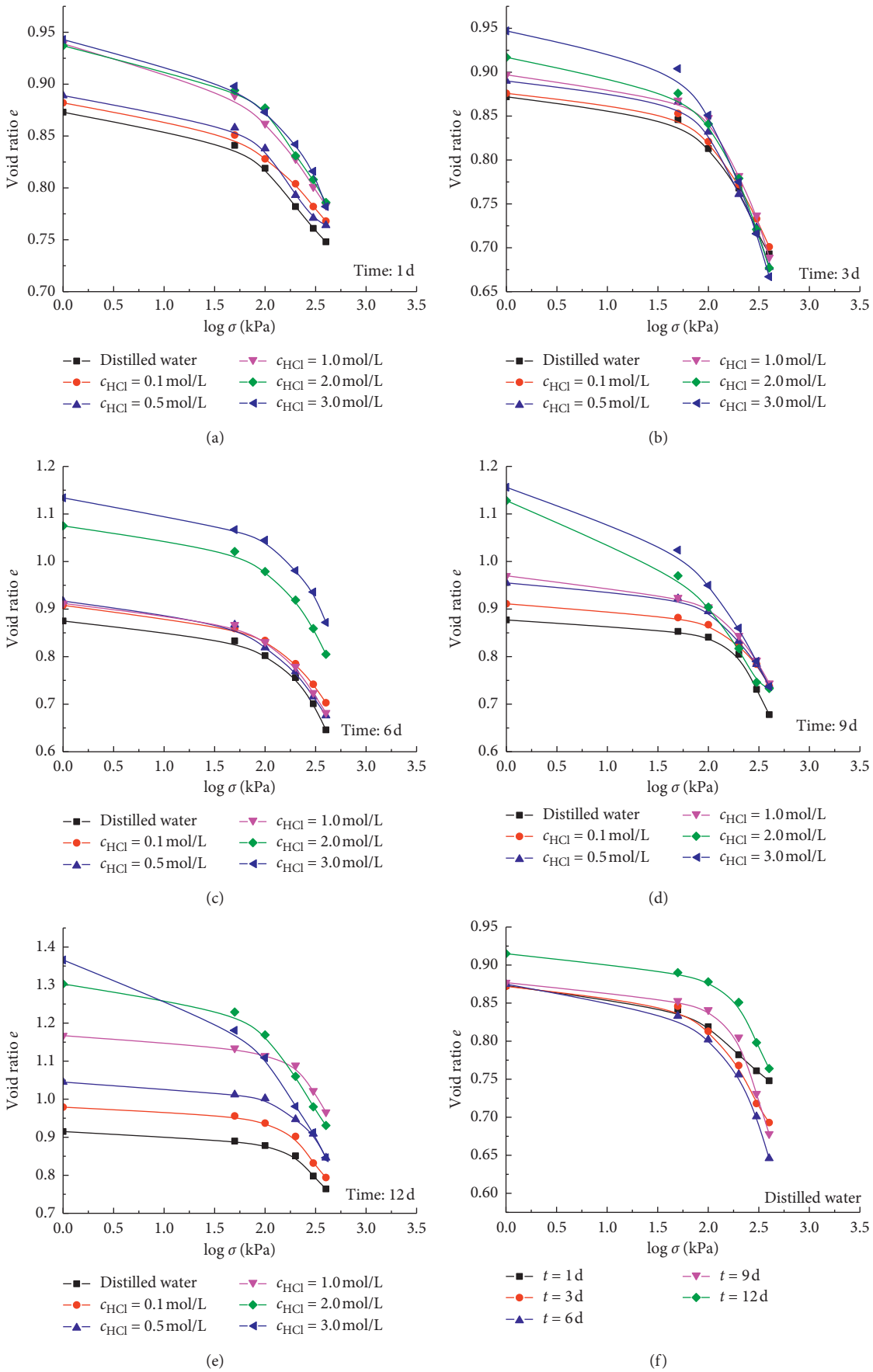

Figure 2: Continued.

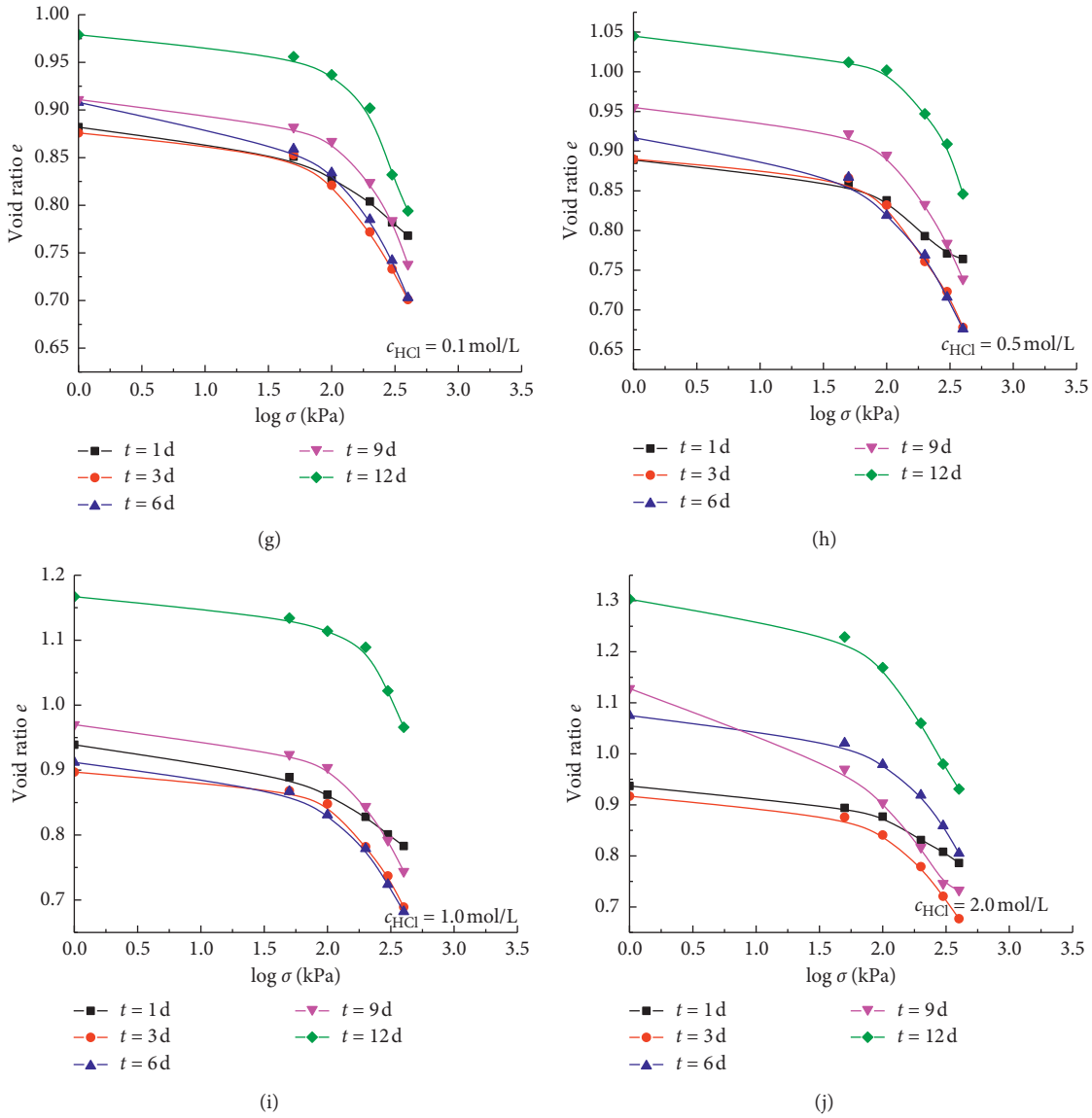

Figure 2: Continued.

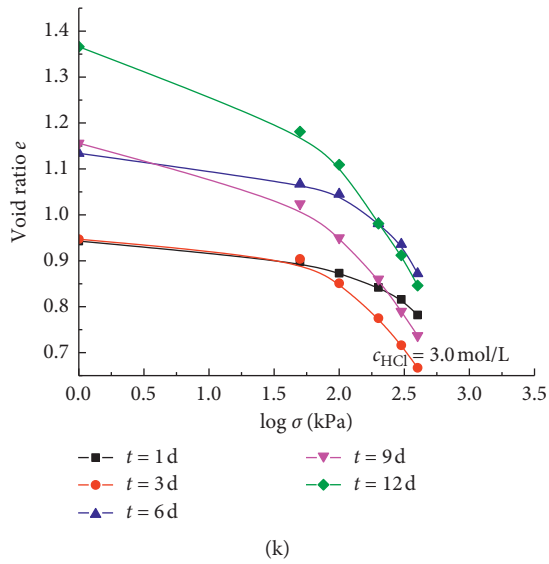

(k)

Figure 2: Compression curve $e - \log \sigma$ of different samples. (a) The acid immersion time is 1 d and the CCC under different acid concentrations. (b) The acid immersion time is 3 d and the CCC under different acid concentrations. (c) The acid immersion time is 6 d and the CCC under different acid concentrations. (d) The acid immersion time is 9 d and the CCC under different acid concentrations. (e) The acid immersion time is 12 d and the CCC under different acid concentrations. (f) The acid concentration is 0 mol/L (distilled water), and the CCC under different acid immersion time. (g) The acid concentration is 0.1 mol/L, and the CCC under different acid immersion time. (h) The acid concentration is 0.5 mol/L, and the CCC under different acid immersion time. (i) The acid concentration is 1.0 mol/L, and the CCC under different acid immersion time. (j) The acid concentration is 2.0 mol/L, and the CCC under different acid immersion time. (k) The acid concentration is 3.0 mol/L, and the CCC under different acid immersion time.

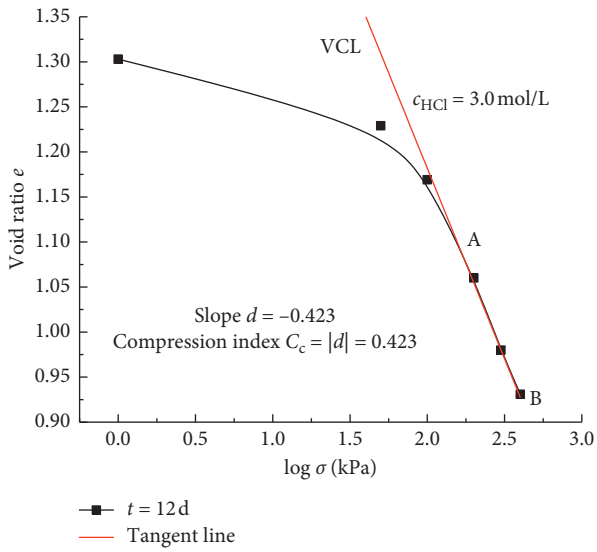

Figure 3: The method of calculating the slope of the compression index C_c.

are solved and combined with the curvature calculation formula to obtain the value of the compressive yield stress (equation (5)).

The value of the compressive yield stress can be calculated using the expression listed in Table 4. The values of the compressive yield stress varied from 48.733 kPa to 128.529 kPa. The data are plotted as a function of the compressive yield stress and the immersion time and acid concentration. As shown in Figure 7, the shapes of the curves

Table 2: Compression index C_c of loess samples under different acid erosion concentrations and times.

c_{HCl} (mol·L^{-1})	Time t (d)				
	1	3	6	9	12
0 (distilled water)	0.112	0.242	0.268	0.279	0.287
0.1	0.118	0.238	0.278	0.298	0.351
0.5	0.126	0.288	0.311	0.319	0.360
1	0.149	0.320	0.324	0.339	0.414
2	0.153	0.341	0.346	0.346	0.423
3	0.210	0.367	0.384	0.411	0.460

are similar, but there are differences. The compressive yield stress value decreased with increasing acid concentration, and the curve gradually followed a decreasing trend as the immersion time increased, indicating that the compressive yield stress value of the sample changed from large to small. It can be concluded that the value of compressive yield stress decreases with the increase in immersion time and acid concentration. The higher the acid concentration, the lower the stress value required to compress a loess specimen for structural failure, and the increase in acid immersion time contributes to this reducing effect.

3.4. SEM Test Results. The images of the undisturbed loess sample and the strong acid corrosion sample (hydrochloric acid concentration 3 mol/L, soaked for 12 days) in the scanning electron microscope at 500x magnification are shown in Figures 8 and 9. As illustrated in Figure 8, a large number of quartz particles are distributed in the undisturbed

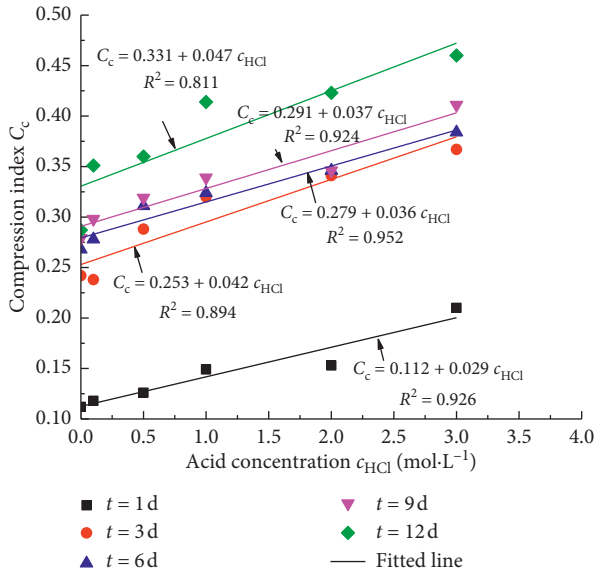

Figure 4: Variation in compression index values with acid concentration.

loess. The particles are in the form of irregular polygons; the surfaces of the particles are relatively flat and smooth, and there are natural pores of different sizes between the particles. After acid corrosion of the loess sample (Figure 9), it is obvious from the figure that there are large corrosion pores on the surface of the soil sample, and there are some sporadic small pores. Compared with the undisturbed loess, the number of pores increased significantly. There were many corrosion holes and corrosion pits on the surface of quartz particles; the particles became small in size, and the surface was rough.

In order to investigate the influence of acidic substances on the pore characteristics of loess, the pore characteristics of loess samples were analyzed using the PCAS image processing software after SEM test. The pore images of the samples were imported (Figure 10(a) for undisturbed loess and Figure 10(d) for acid-etched loess), and the pore images of the samples were binarized. The white area represents pores, and the black area represents particles. The following text describes the method of calculation [34, 35].

As for the classification of micropores in rock and soil mass, scholars have adopted different classification standards. [36, 37] The pores of acid etched loess are classified statistically by using the classification method of scholar Lei [38].

The pores of the soil were divided into the following four types according to the radius and microporosity ($0\,\mu m < R \le 1\,\mu m$), small pores ($1\,\mu m < R \le 4\,\mu m$), medium pores ($4\,\mu m < R \le 16\,\mu m$), and large pores ($R > 16\,\mu m$). Figure 11 provides the relationship between the distribution of the number of pores and area ratios of different sizes of the original loam and acid-etched loam, corresponding to the line and histogram, respectively. From the pore number distribution line diagram, the curve of the acid-etched loam is above the original loam, in the range of microporosity (0-1 μm); the number of microporosities of the acid-etched loam is 149, the number of microporosities of the original loam is 39, in the range of small pores (1–4), the number of small pores in the acid-etched loess is 307, the number of small pores in the original loess is 49, the number of medium pores in the range of medium pores (4–16 μm), the number of medium pores in the acid-etched loess is 1, the number of medium pores in the original loess is 0, the number of large pores in the range of large pores (>16 μm), the number of large pores in the acid-etched loess is 3, and the number of large pores in the original loess is 0. It can be seen that the number of pores in the sample of loess etched by acid solution increased significantly; in particular, the number of micropores and small pores increased by a large amount (0–4 μm); the acid-etched loess was also present in 3 pores of larger diameter, which indicated that there was an interaction between the acidic substances and soil; further, this also indicated a chemical corrosion reaction that caused small soluble substances from the loess body, thus forming a large number of small pores. Moreover, these small pores not only existed, but also formed many small pores between particles. When an increasing number of small pores are produced on the surface of the particles, under the action of acidic solutions and their own gravity, the pore walls between the small pores gradually disappear; this leads to the conversion of small pores into larger pores, resulting in obvious dissolution of small pores.

From the histogram of the pore area of each pore diameter, we can see that the original loess pores are mainly distributed in the range of pore diameters of micropores and small pores. In this case, the micropore area accounts for 20.90% of the total area of the original loess pore; the small pore area accounts for 79.10% of the total area of the original loess pore. Further, the acid-etched loess pores are distributed in the micropores, small pores, medium pores, and large pores, in which the small pore area accounted for 37.21%, the medium pore area accounted for 1.14%, and the large pore area accounted for 55.41%. For each pore diameter, the pore area ratio data reflect that the original loess sample with small pore occupies the largest area, and the acid-etched loess large pore area accounted for the most, indicating that after the action of acidic substances of the loess body the pore area of large pores gradually increased the proportion of the pore area. The acidic material reacts with the loess body and gradually expands the original small pores into large pores. The acid-etched loess with many pores was compressed under different vertical loads, and the large pores were compressed and destroyed by the load, and the small pores gradually contracted.

In this study, we investigated the effect of acid concentration and immersion time on the compressibility of loess from the point of view that acid may affect the mechanical properties of loess. Six concentrations were selected in the range of 0–3 mol/L hydrochloric acid, and the immersion time was set from 1 to 12 days, and the specimens were taken out at 1, 3, 6, 9, and 12 days for the confined compression test. The compressibility of acid-etched loess is enhanced compared to the original loess, and the enhancement magnitude is related to the immersion time and acid concentration.

Table 3: The linear fitting equation for the compression index C_c, soaking time, and acid concentration.

Acid soaking time t (d)	Linear fitting equation	R^2	Acid concentration c_{HCl} (mol·L^{-1})	Linear fitting equation	R^2
1	$C_c = 0.112 + 0.029c_{HCl}$	0.926	0 (distilled water)	$C_c = 0.156 + 0.013t$	0.652
3	$C_c = 0.253 + 0.042c_{HCl}$	0.894	0.1	$C_c = 0.143 + 0.018t$	0.858
6	$C_c = 0.279 + 0.036c_{HCl}$	0.952	0.5	$C_c = 0.175 + 0.017t$	0.700
9	$C_c = 0.291 + 0.037c_{HCl}$	0.924	1	$C_c = 0.192 + 0.019t$	0.741
12	$C_c = 0.331 + 0.047c_{HCl}$	0.811	2	$C_c = 0.206 + 0.019t$	0.677
N/A	N/A	N/A	3	$C_c = 0.250 + 0.019t$	0.778

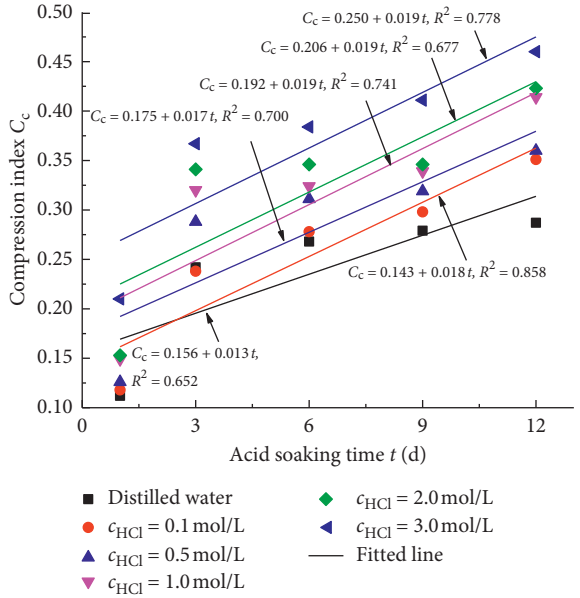

Figure 5: Compression index C_c changes with immersion time.

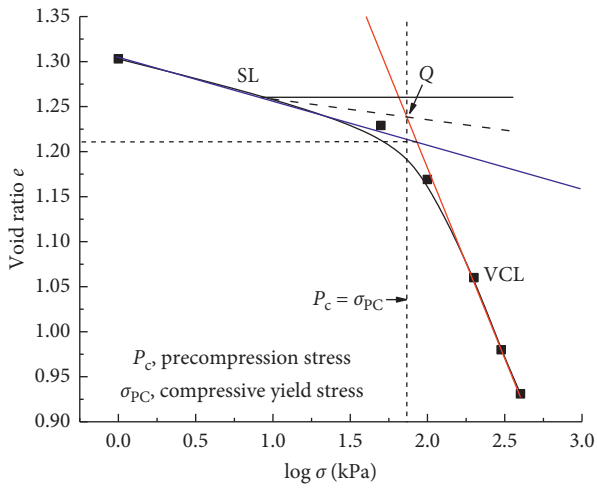

Figure 6: Calculation of compressive yield stress σ_{pc} by intersection method.

The macroscopic compressive mechanical property of acid-etched loess may be related to the change of the number and area of microscopic pores, and the results meet the ideal expectation. The test results show that when the soaking time is the same, the hydrochloric acid concentration increases from 0 to 3.0 mol/L, the compression coefficient C_c increases

Table 4: Compressive yield stress σ_{pc} of loess samples under different acid erosion concentration and time.

c_{HCl} (mol·L^{-1})	Time t (d)				
	1	3	6	9	12
0 (distilled water)	128.529	130.918	126.183	126.009	100.231
0.1	98.628	96.605	92.470	89.331	85.114
0.5	89.125	85.310	84.333	81.846	79.616
1	72.946	70.795	69.502	66.527	61.518
2	73.282	72.778	69.663	52.481	53.951
3	56.624	54.325	50.933	49.317	48.753

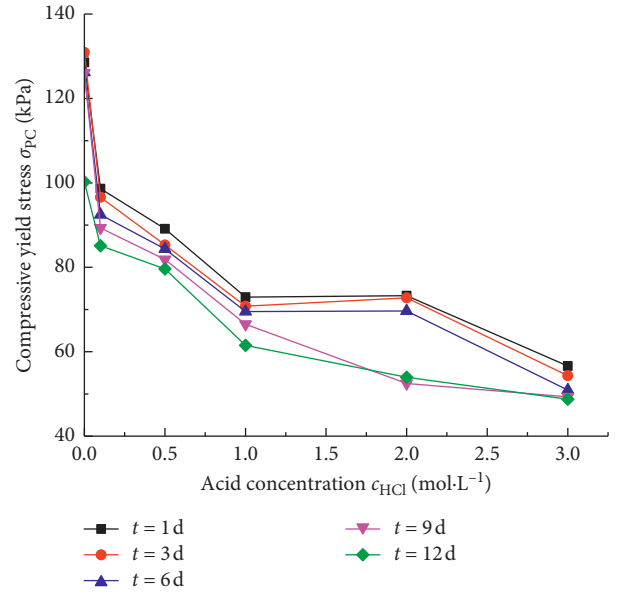

Figure 7: Compression yield stress change curve.

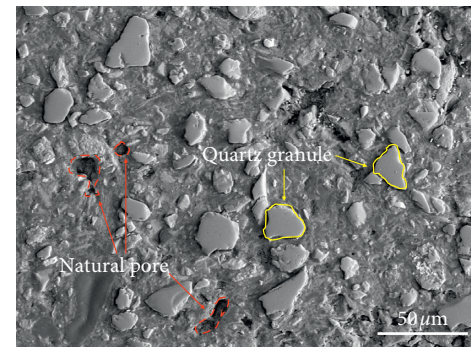

Figure 8: Original scanning electron microscope image of undisturbed loess (magnified 500x).

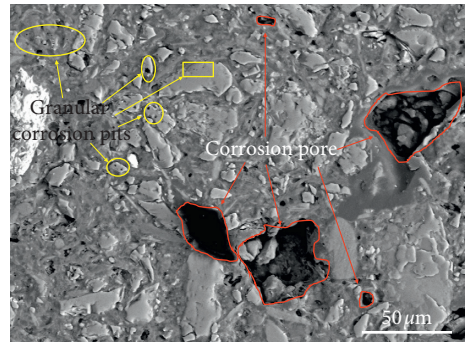

Figure 9: Original scanning electron microscope image of acid-etched loess (magnified 500x), HCl concentration 3 mol/L, and immersion time of 12 days.

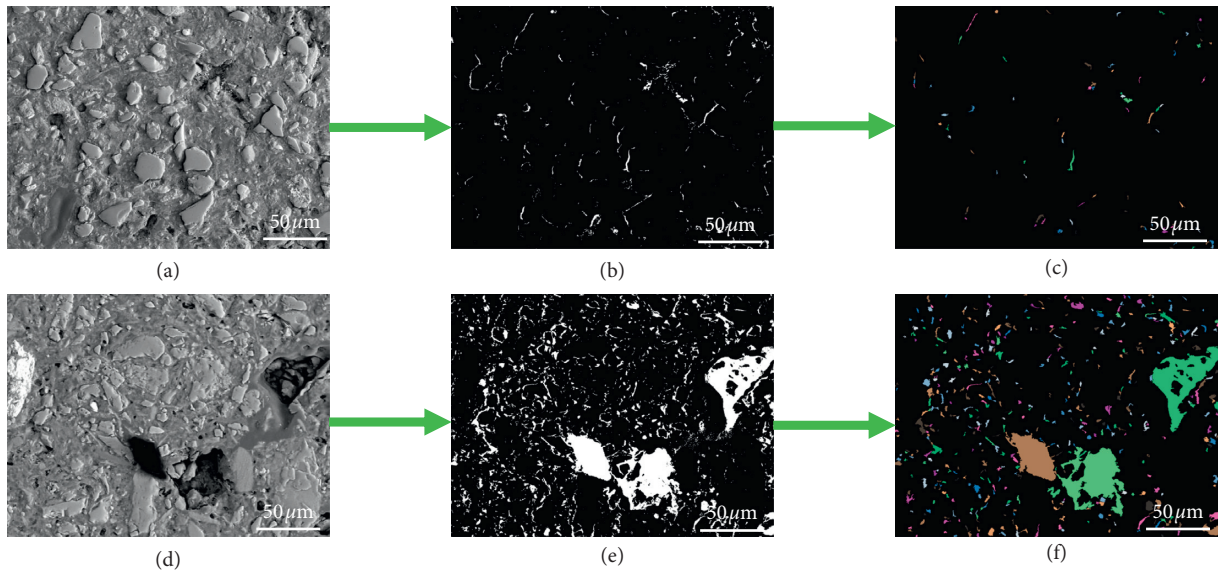

Figure 10: Binarization and pore extraction of microscopic images of loess specimens. SEM images of undisturbed loess: (a) original, (b) with binary image processing, and (c) with vectorization. SEM images of acid-etched loess: (d) original, (e) with binary image processing, and (f) with vectorization.

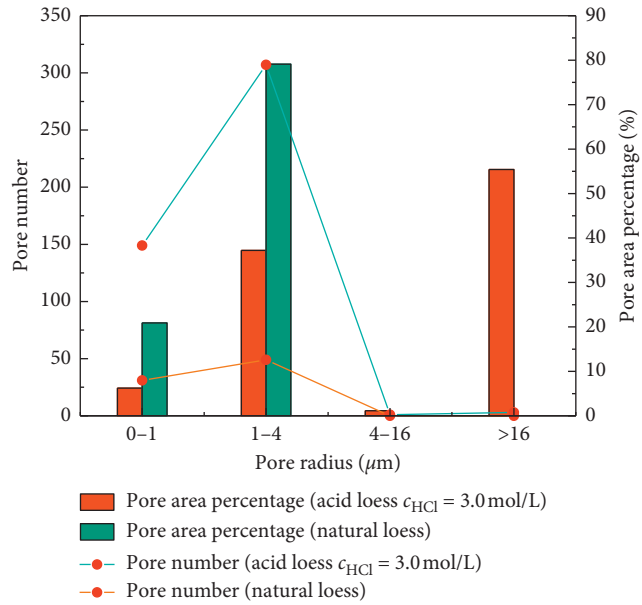

Figure 11: Variation of sample pore characteristics.

by 43.20–87.5%, and the compression yield stress σ_{pc} decreases by 51.36–60.86%; when the concentration of hydrochloric acid is the same, the soaking time increases from 1 day to 12 days, the compression coefficient C_c increases by 119.05–197.46%, and compressive yield stress σ_{pc} decreases by 10.67–22.02%. The microscopic images of loess soaked for 12 days at 3.0 mol/L hydrochloric acid concentration were compared with those of the original loess. The percentages of micropore, small pore, mesopore, and macropore areas of original loess were 20.90%, 79.10%, 0%, and 0%, respectively. The percentages of areas of acid-etched loess were 6.24%, 37.21%, 1.14%, and 55.40%, respectively. The enhancement of the compressive properties of acid-etched loess is the result of the coupling of acid concentration and soaking time, and the change of macroscopic compressive properties may be related to the increase of microscopic macropore area after acid erosion.

Loess contains a large number of salts and calcium carbonate, and when the acid enters the loess, it reacts chemically with these substances. The greater the concentration of acid and the longer the immersion time, the fuller the chemical reaction, the more the salts and calcium carbonate in the loess are dissolved and the pores of the loess gradually become larger. In this study, the soil compressibility is enhanced under external load, and the degree of enhancement may be related to the degree of acid corrosion. In the present study, the enhancement of macroscopic compressibility was investigated only by microscopic scanning electron microscopy (SEM), and the next step is to investigate the changes of chemical composition of loess by acid. The results of this study can provide a reference for the study of mechanical properties and engineering construction of foundation soils in acid-contaminated areas, which is of great theoretical and engineering significance.

4. Conclusion

By simulating the acid-contaminated loess specimens in an indoor test, the compression test of acid-contaminated specimens was conducted to investigate the characteristics of the compression curve and compression index, compression yield stress, and other indicators of compression characteristics of loess under the influence of two factors, namely, changes in acid concentration and acid immersion time. Further, the scanning electron microscope images of acid-contaminated loess and original loess specimens were obtained. From the test results and data analysis results, the following conclusions can be drawn:

(1) The value of the initial porosity ratio e_0 of the acid-corroded loess increases with increasing acid concentration, and the longer the acid immersion time, the larger the initial porosity ratio e_0. The CCC curves of acid-etched loess have similar morphology, and the greater the acid concentration and the longer the immersion time, the higher the position of the CCC.

(2) The compressive index C_c was positively correlated with the acid concentration. The compressive index C_c was also positively correlated with the increase in soaking time from 1, 3, 6, 9, and 12 days. The compressive yield stress in the acid-corroded loess decreased gradually with increasing acid concentration and soaking time. The enhanced compressive property of the acid-corroded loess was the result of the coupling effect between the increase in acid concentration and the increase in soaking time.

(3) Compared with the original loess, the number of micropores and small pores in acid-etched loess increased, and the pores not only existed between the particles, but also had pits and even small pores on the surface of the particles, as well as large erosion holes. The appearance of these pores and holes may be related to the increase of compression coefficient and decrease of compressive yield stress in acid-erosion loess, which may be the main reason for the increase of compressibility of acid-erosion loess.

Data Availability

The data used to support the findings of this study are available from the corresponding author upon request.

Conflicts of Interest

The authors declare that they have no conflicts of interest.

Acknowledgments

This work was financially supported by the National Natural Science Foundation of China (Grant nos. 41602305 and 41572287) and the Basic Research Program of Natural Science of Shaanxi Province (2020JQ-745). The authors offer their gratitude and regards to the colleagues who contributed to this work.

References

[1] T. A. Dijkstra, C. D. F. Rogers, I. J. Smalley et al., "The loess of north-central China: geotechnical properties and their relation to slope stability," *Engineering Geology*, vol. 36, no. 3-4, pp. 153–171, 1994.

[2] H. M. Roberts, D. R. Muhs, and E. Lii, "Loess records | North America," *Encyclopedia of Quaternary Science*, vol. 266, pp. 620–628, 2013.

[3] M. A. Zárate, "Loess records | south America," *Encyclopedia of Quaternary Science*, vol. 26, no. 6, pp. 629–641, 2007.

[4] R. G. Gimenez, R. V. D. L. Villa, and J. A. G. Martin, "Characterization of loess in central Spain: a microstructural study," *Environmental Earth Ences*, vol. 65, no. 7, pp. 2125–2137, 2012.

[5] D. R. Muhs, "Loess deposits: origins and properties," *Encyclopedia of Quaternary Ence*pp. 573–584, Elsevier, Amsterdam, Netherlands, 2nd edition, 2013.

[6] E. Derbyshire, T. A. Dijkstra, I. J. Smalley, and Y. Li, "Failure mechanisms in loess and the effects of moisture content changes on remoulded strength," *Quaternary International*, vol. 24, pp. 5–15, 1994.

[7] E. Derbyshire, "Geological hazards in loess terrain, with particular reference to the loess regions of China," *Earth Ence Reviews*, vol. 54, no. 1–3, pp. 231–260, 2011.
[8] J. Palmer, "Creeping earth could hold secret to deadly landslides," *Nature*, vol. 548, no. 7668, pp. 384–386, 2017.
[9] M. Sun, H. Tang, M. Wang et al., "Creep behavior of slip zone soil of the majiagou landslide in the three gorges area," *Environmental Earth Sciences*, vol. 75, no. 16, p. 1199, 2016.
[10] X. Wang, Y. Yin, J. Wang, B. Lian, H. Qiu, and T. Gu, "A nonstationary parameter model for the sandstone creep tests," *Landslides*, vol. 15, no. 7, pp. 1377–1389, 2018.
[11] T. Keller and J. Arvidsson, "Compressive properties of some Swedish and Danish structured agricultural soils measured in uniaxial compression tests," *European Journal of Soil Ence*, vol. 58, no. 6, pp. 1373–1381, 2010.
[12] T. Keller, J. Arvidsson, J. B. Dawidowski et al., "Soil precompression stress," *Soil and Tillage Research*, vol. 77, no. 1, pp. 97–108, 2004.
[13] K. M. V. Cavalieri, J. Arvidsson, A. P. da Silva, and T. Keller, "Determination of precompression stress from uniaxial compression tests," *Soil and Tillage Research*, vol. 98, no. 1, pp. 17–26, 2008.
[14] A. J. Koolen, H. Kuipers, Agricultural soil mechanics, 1986, in Japanese.
[15] T. Baumgartl and B. Köck, "Modelling volume change and mechanical properties with hydraulic models," *Soil Ence Society of America Journal*, vol. 68, no. 1, 2004.
[16] S. Imhoff, A. P. Da Silva, and D. Fallow, "Susceptibility to compaction, load support capacity, and soil compressibility of hapludox," *Soil Science Society of America Journal*, vol. 68, no. 1, pp. 17–24, 2004.
[17] H. L. Kuan, P. D. Hallett, B. S. Griffiths et al., "The biological and physical stability and resilience of a selection of scottish soils to stresses," *European Journal of Soil Science*, vol. 58, no. 3, pp. 811–821, 2010.
[18] K. Saffih-Hdadi, P. Défossez, G. Richard, Y.-J. Cui, A.-M. Tang, and V. Chaplain, "A method for predicting soil susceptibility to the compaction of surface layers as a function of water content and bulk density," *Soil and Tillage Research*, vol. 105, no. 1, pp. 96–103, 2009.
[19] S. V. Sivapriya, S. Rajagopalan, A. Duraimurugan et al., "Physiochemical properties of contaminated soil under the influence of industrial and municipal wastewater," *International Journal of Environmental Ence and Technology*, vol. 17, no. 11, 2020.
[20] S. M. Khodary, A. M. Negm, and A. Tawfik, "Geotechnical properties of the soils contaminated with oils, landfill leachate, and fertilizers," *Arabian Journal of Geosciences*, vol. 11, no. 2, 2018.
[21] C. Li, G. Sun, Z. Wu et al., "Soil physiochemical properties and landscape patterns control trace metal contamination at the urban-rural interface in southern China," *Environmental Pollution*, vol. 250, pp. 537–545, 2019.
[22] L. M. Shekhtman, V. T. Baranov, and G. F. Nesterenko, "Building deformations caused by the leakage of chemical reagents," *Soil Mechanics and Foundation Engineering*, vol. 32, no. 1, pp. 32–36, 1995.
[23] K. Kobeticova and R. Cerny, "Ecotoxicology of building materials: a critical review of recent studies," *Journal of Cleaner Production*, vol. 165, no. 1, pp. 500–508, 2017.
[24] M. Oenal, "Swelling and cation exchange capacity relationship for the samples obtained from a bentonite by acid activations and heat treatments," *Applied Clay Ence*, vol. 37, no. 1-2, pp. 74–80, 2007.
[25] B. Tyagi, C. D. Chudasama, and R. V. Jasra, "Determination of structural modification in acid activated montmorillonite clay by ft-ir spectroscopy," *Spectrochimica Acta Part A: Molecular and Biomolecular Spectroscopy*, vol. 64, no. 2, pp. 273–278, 2006.
[26] S. A. Gregory, W. R. Whalley, C. W. Watts, N. R. A. Bird, P. D. Hallett, and A. P. Whitmore, "Calculation of the compression index and precompression stress from soil compression test data," *Soil & Tillage Research*, vol. 89, no. 1, pp. 45–57, 2006.
[27] ASTM C496/C496M, *Standard Test Method for Splitting Tensile Strength of Cylindrical Concrete Specimens*, ASTM International, West Conshohocken, PA, USA, 2017.
[28] BS1377, *Methods of Test for Soils for Civil Engineering Purposes - Part 8: Shear Strength Tests (Effective Stress)*, British Standards Institution, London, UK, 1990.
[29] GB/T 50123, *Standard Test for Soil Test Method*, China Planning Press, Beijing, China, 1999.
[30] B. Gompertz, C.-S. Tang, B. Shi, and W.-B. Suo, "On the nature of the function expressive of the law of human-mortality, and on a new mode of determining the value of life contingencies." *Philosophical Transactions of the Royal Society of London*, vol. 115, pp. 513–585, 1825.
[31] A. Casagrande, *Determination of the pre-consolidation load and its practicalsignificance*, pp. 60–64, Proceedings of the International Conference on the Soil Mechanics and Foundation Engineering, Cambridge, UK, June 1936.
[32] C. Liu, B. Shi, J. Zhou, and C. Tang, "Quantification and characterization of microporosity by image processing, geometric measurement and statistical methods: application on sem images of clay materials," *Applied Clay Science*, vol. 54, no. 1, pp. 97–106, 2011.
[33] C. Liu, C.-S. Tang, B. Shi, and W.-B. Suo, "Automatic quantification of crack patterns by image processing," *Computers & Geosciences*, vol. 57, pp. 77–80, 2013.
[34] J. F. Liu, X. L. Cao, J. Xu et al., "A new method for threshold determination of gray image," *Geomechanics and Geophysics for Geo-Energy and Geo-Resources*, vol. 6, no. 4, 2020.
[35] S. B. Song, J. F. Liu, H. Y. Ni et al., "A new automatic thresholding algorithm for unimodal gray-level distribution images by using the gray gradient information," *Journal of Petroleum Science and Engineering*, vol. 190, pp. 1–7, 2020.
[36] J. F. Liu, S. B. Song, X. L. Cao et al., "Determination of full-scale pore size distribution of Gaomiaozi bentonite and its permeability prediction," *Journal of Rock Mechanics and Geotechnical Engineering*, vol. 12, no. 2, pp. 195–205, 2020.
[37] R. G. Loucks, R. M. Reed, S. C. Ruppel, and U. Hammes, "Spectrum of pore types and networks in mudrocks and a descriptive classification for matrix-related mudrock pores," *Aapg Bulletin*, vol. 96, no. 6, pp. 1071–1098, 2012.
[38] X. Y. Lei, "Pore types and collapsibility of loess in China," *Science in China*, vol. 17, no. 12, pp. 1209–1318, 1987.